

# Electrically Switchable Photonic Molecule Laser

Gernot Fasching,<sup>1,2</sup> Christoph Deutsch,<sup>1,2</sup> Alexander Benz,<sup>1,2</sup> Aaron Maxwell Andrews,<sup>3,2</sup> Pavel Klang,<sup>3,2</sup> Reinhard Zobl,<sup>3</sup> Werner Schrenk,<sup>3,2</sup> Gottfried Strasser,<sup>3,2</sup> Paulius Ragulis,<sup>4</sup> Vincas Tamošiūnas,<sup>4</sup> and Karl Unterrainer<sup>1,2</sup>

<sup>1</sup>Photonics Institute, Vienna University of Technology, Gusshausstrasse 27/387, 1040 Wien, Austria

<sup>2</sup>Centre for Micro- and Nanostructures, Vienna University of Technology, Florag. 7, 1040 Wien, Austria

<sup>3</sup>Institute of Solid-State Electronics, Vienna University of Technology, Florag. 7, 1040 Wien, Austria

<sup>4</sup>Semiconductor Physics Institute, A. Gostauto 11, 01108 Vilnius, Lithuania

We have studied the coherent intercavity coupling of the evanescent fields of the whispering gallery modes of two terahertz quantum-cascade lasers implemented as microdisk cavities. The electrically pumped single-mode operating microcavities allow to electrically control the coherent mode coupling for proximity distances of the cavities up to 30-40  $\mu\text{m}$ . The optical emission of the strongest coupled photonic molecule can be perfectly switched by the electrical modulation of only one of the coupled microdisks. The threshold characteristics of the strongest coupled photonic molecule demonstrates the linear dependence of the gain of a quantum-cascade laser on the applied electric field.

PACS numbers:

In general, photons couple much less with respect to electrons allowing photonic circuits to be faster, providing more bandwidth and having lower power consumption compared to their electronic counterparts. Merging optics and electronics for future optical circuits<sup>1,2</sup> is still an open challenge mainly due to the lack of a chip based platform providing photon sources and manipulation units at once. Hybrid solutions are on the way<sup>3,4</sup> to bridge between sources and circuits, but the efficient coupling into photonic circuits remains still a problem to be overcome. The III-V material system is well suited for fully functional optoelectronics, as it combines both optical and electronic functions. GaAs based compact and unipolar mid-infrared<sup>5</sup> and terahertz (THz)<sup>6</sup> emitting lasers called quantum-cascade lasers (QCLs) have already been realized. The light amplification is based on intersubband (ISB) transitions, i.e. transitions between one-dimensional quantized energy levels within one band of a cascaded semiconductor heterostructure. Quantum-cascade microlasers with in-plane highly directional<sup>7</sup>, in-plane unidirectional<sup>8</sup>, or surface<sup>9,10</sup> emission as well as active photonic crystals<sup>11,12,13</sup> have also been established, providing the basic building blocks for light manipulation and waveguiding. Hence, photon sources and waveguides are already established in the THz spectral range, but the optical intercavity coupling has not been studied so far.

In this Letter we investigate for the first time the electrically controlled coherent optical coupling between two whispering-gallery modes (WGMs), which is based on phase and mode matched power exchange of the constituting fields. Hence, by the linear combination of the optical fields of microdisk lasers one can create so called photonic molecules<sup>14</sup> (PMs). Compared to former realizations of PMs, e.g. microspheres<sup>15,16</sup> or semiconductor microcavities<sup>14,17</sup>, PMs based on microdisk THz-QCLs differ in several important aspects from these approaches. First, THz-PMs comprise an electrically pumped optical gain enabling fast electrically controlled mode tuning and switching. Second, the plasmonic mode confinement per-

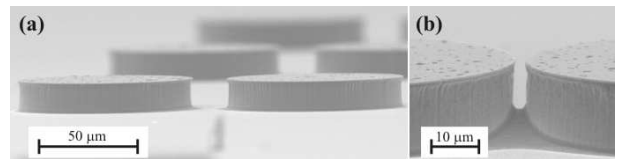


Figure 1: Scanning electron micrograph images of double-metal microdisks forming electrically tunable THz photonic molecules with a proximity spacing of (a) 12 (PM-12) and (b) 2  $\mu\text{m}$  (PM-2).

mits sub-wavelength sized cavities. This allows to study the optical coupling of just two single modes and the precise control over the resonance frequency. And third, the combination of gain switching and exact spatial cavity configuration offers a precise control over the resulting mode configuration and on chip integration.

The investigated PMs consist of two THz-QCLs having each a cylindrical resonator as shown in Fig. 1, i.e. a microdisk cavity, with the same nominal dimensions of radius  $R=45 \mu\text{m}$  and height  $H=16.2 \mu\text{m}$ . The varying proximate spacings between the microdisks result in different coupling strengths. The proximate spacing  $x$  will be included in the terminology as PM- $x$ .

The active gain region of the microdisks is based on a four well/barrier GaAs/ $Al_{0.15}Ga_{0.85}As$  heterostructure<sup>18</sup>, which has been repeated 271 times during the growth to achieve a large modal gain. The heterostructure is embedded between two metal layers serving as electrical contacts and allowing for strong vertical mode confinement ( $\lambda \gg H$ ), whereas the lateral confinement is provided by the impedance mismatch between the gain material and the air. Details of the design, growth, and processing can be found elsewhere<sup>8</sup>. The field dependent emitted optical power of the PMs has been measured in a closed light pipe equipped with a Ga doped Ge (Ge:Ga) detector. The PMs were operated in pulsed-mode with 100 ns short pulses and double modulated at 100 Hz with a duty-cycle of 50 % to allow

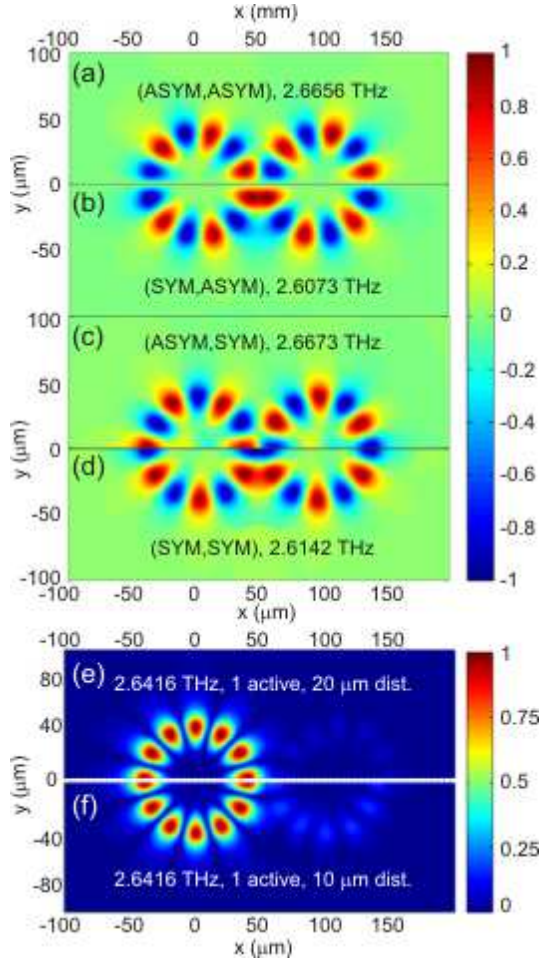


Figure 2: Spatial field distributions of the  $z$  component of the electric field. (a-d) The sign of the real part of the amplitude is assigned to the absolute value of the amplitude in order to indicate the phase differences of the restricted symmetric and antisymmetric simulations in the case of a PM-2. (e,f) Full area simulations of a PM-20 and a PM-10 having only one active microdisk. In both molecules the lasing mode couples into the passive cavity.

for the detection with a Ge:Ga detector. The light pipe was immersed in liquid helium, such that room temperature background radiation could not distort the measurements.

Full 3-D finite-difference time-domain (FDTD) simulations have been performed to reveal the properties of PM modes. A custom-made code<sup>19</sup> was employed for this purpose, which includes several enhancements over the classical FDTD, such as a Maxwell-Bloch module for two-level quantum systems. In addition to full-window simulations<sup>20</sup>, higher resolution simulations were performed with restricted symmetry to reveal the detailed field configurations. The modes are labelled by a pair  $(x, y)$ , indicating a symmetric (SYM) or antisymmetric (ASYM) field configuration with respect to the symmetry planes perpendicular ( $x$ ) or parallel ( $y$ ) to the molecule axis.  $(ASYM, y)$  modes are *pushed* further inside the

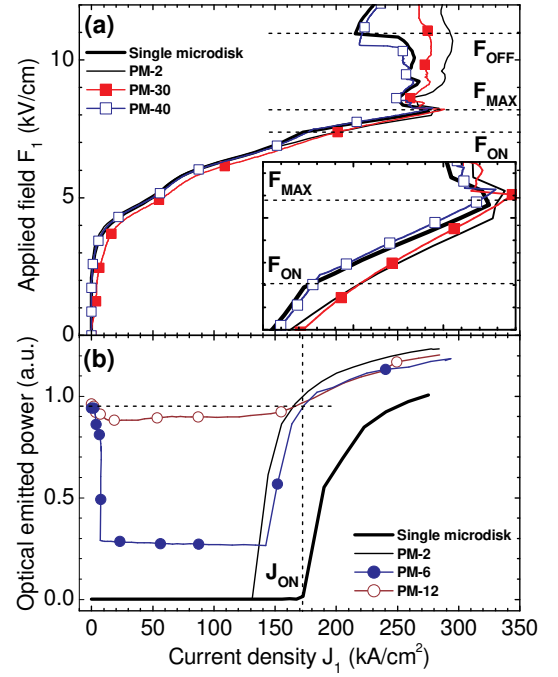


Figure 3: (a) The current density-applied field ( $J - F$ ) characteristics of a single microdisk and several PMs at  $T=5$  K. The applied electric fields at the lasing onset, at the maximum lasing emission, and at the end of the lasing emission of a single microdisk are labelled  $F_{ON}$ ,  $F_{MAX}$  and  $F_{OFF}$ , respectively. The applied field of the second microdisk of each PM was kept constant at  $F_{const}=(F_{ON}+F_{MAX})/2$ . The inset depicts a blow up of the  $J - F$  characteristics between  $F_{ON}$  and  $F_{MAX}$  to clarify the increase in current for the PM-2 and the PM-30 within this region. (b) The current density-optical emitted power characteristics of a single microdisk and several PMs at  $T=5$  K. The dashed horizontal line mark the lasing emission of the PM-6 and PM-12 for  $J_1=0$ . The dashed vertical line mark the threshold current density  $J_{ON}$  of a single microdisk.

resonator compared to  $(SYM, y)$  modes, resulting in different effective optical paths causing higher emission frequencies for the  $(ASYM, y)$  modes as shown in Fig. 2(a-d). For the case of one active and one passive/absorbing microdisk as shown for a PM-20 and a PM-10 in Fig. 2(e,f), the mode is well localized in the active cavity but couples also into the passive cavity. Hence, the operation of a PM is tunable by changing the effective loss of the passive cavity.

The optical intercavity coupling between microdisks forming a PM has a strong impact on the electrical and optical characteristics as shown in Fig. 3. A single, uncoupled microdisk exhibits the typical current density-applied field characteristics due to ISB tunneling and lasing emission<sup>21</sup>, i.e. a kink at the onset of the lasing emission and a negative differential resistivity regime above the maximum lasing emission labelled  $F_{ON}$  and  $F_{MAX}$  in Fig. 3(a), respectively. Compared to that, the PM-2 and the PM-30 exhibit higher current densities starting

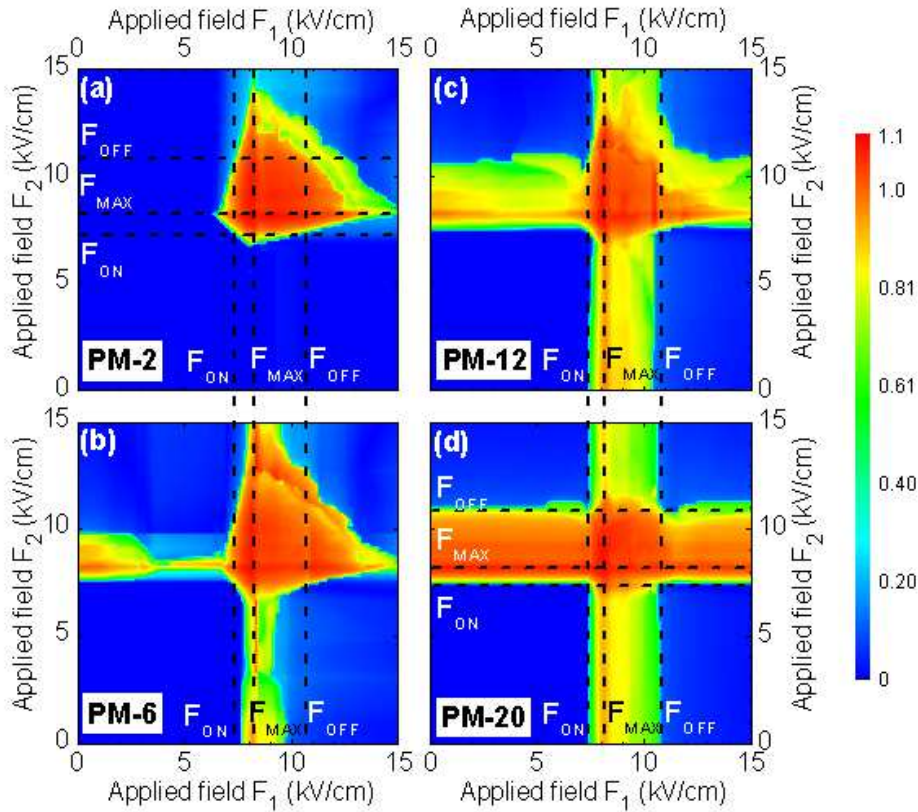


Figure 4: The optical emitted power of four PMs as a function of the applied electric fields with decreasing intercavity coupling from (a) to (d). The dashed horizontal and vertical lines labelled  $F_{ON}$ ,  $F_{MAX}$ , and  $F_{OFF}$ , respectively, mark the applied electric fields at the lasing onset, the maximum lasing emission, and at the end of the lasing emission of a single, uncoupled microdisk.

below  $F_{ON}$  up to well above  $F_{OFF}$ . This is a consequence of the strong *optical* intercavity coupling causing the additional photon enhanced current flow. The PM-40 does not show such an increase indicating that the strong optical coupling is limited to  $\approx 30\text{-}40 \mu\text{m}$ .

Fig. 3(b) shows the optical emitted power of a single microdisk and several PMs. The PM-2 depicts the same qualitative behaviour and the same threshold current density  $J_{ON}$  of a single microdisk, i.e.  $J_1 + J_2 = 2J_{ON}$ , reflecting that a PM-2 acts as a *single* cavity QCL.

The PM-6 and the PM-12 exhibit emission already at  $J_1 = 0$ , i.e. the single peak gain of the second microdisk is larger than the loss of the coupled system. The emission of these PMs is decreasing around  $J_1 \approx 10 \text{ A/cm}^2$  due to carrier injection into the other microdisk leading to ISB absorption. The lasing emission of these PMs recover exactly at  $J_1 = J_{ON}$ , i.e. the additional loss is balanced by the gain.

Fig. 4 shows the electrical control of the lasing emission of four PMs. The unique possibility to externally control the gain/loss of each cavity of a PM allows to tune the spatial mode configuration. The strongest coupled system shown in Fig. 4(a) lases only if both cavities provide gain. This electrically controlled purely optical conditional switching represents a logical AND opera-

tion. All weaker coupled systems exhibit lasing also if only one microdisk is biased beyond the lasing threshold field  $F_{ON}$ , which is an equivalent to a logical OR operation. Adding a NOT operation by electrically inverting the applied field of a single microdisk completes the set of necessary basic operations, i.e. a logical AND, OR, and NOT, to perform all possible Boolean operations. This demonstrates, that a network of optically coupled THz laser can be utilized to perform any complex logical operation.

The general transition from the strongly to the weakly coupled PM by increasing the spacing between the microdisks from 2 to 20  $\mu\text{m}$  is directly reflected by the change from the trapezoid-shaped to the cross-shaped lasing emission.

The onset of the optical emission of the PM-2 is linearly and equally dependent on the applied electric fields  $F_1$  and  $F_2$  below  $F_{MAX}$ , i.e. below the onset of the negative differential resistivity regime. Hence, (i) the gain of a *single* THz-QCL is linear proportional to the applied field above as well as below the threshold with the *same* slope<sup>22</sup> and (ii) the alignment of the energy levels is achieved well before the lasing threshold field  $F_{ON}$ . The onset of the gain reduction beyond  $F_{MAX}$  requires both applied fields to increase linearly to maintain lasing

emission. Thus, the gain of a *single* THz-QCL is also linear proportional to the applied field above  $F_{MAX}$ , i.e. in the negative differential resistivity regime. The lasing emission of the PM-2 molecule extends beyond  $F_{OFF}$  and is limited by the onset of the gain reduction in the other microdisk at  $F_{MAX}$ .

The decrease in coupling efficiency allows for additional lasing regions between  $F_{ON}$  and  $F_{OFF}$  as shown in Fig. 4(b-d). The lasing emission in Fig. 4(b) is strongly dependent for  $F_1 \approx 3.7$  kV/cm. As discussed in Fig. 3(b), the injected carriers in the other microdisk cause an increase in absorption of the optically coupled system. The increase of the spacing to  $12 \mu\text{m}$  leads to a pronounced increase of the single microdisk lasing areas extending the available lasing range. Finally, the optical emission of the PM-20 shown in Fig. 4(d) covers almost only the whole applied electric field range of two independent microdisks between  $F_{ON}$  and  $F_{OFF}$ . Hence, the crossed-like emission indicates the strong reduction of the mutual coupling.

In summary, we have demonstrated the coherent evanescent coupling of two THz emitting microdisk lasers representing a PM. The electrical characteristics demonstrate mutual coupling up to 30-40  $\mu\text{m}$  intercavity spacing which is comparable to the intracavity lasing wave-

length. As a consequence of carrier lifetimes in the picosecond range THz-PMs can be operated with 100 ns short pulses performing extremely fast electrically gated optical modulation as well as logical AND and OR operations. The characteristics of the optical emitted power demonstrate a linear control of the ISB gain by the applied electric field.

THz emitting PMs might have a great potential for sub-wavelength photonic devices which can be easily realized by standard lithography. Hence, they might find their way into photonics as applications for highly sensitive gas sensors using the evanescent coupled fields with electrical readout or coherently coupled laser arrays with vertical outcoupling for power emission and possible beam shaping and steering. On chip integration of these electrically controllable discrete elements as couplers, filters, gates or flip-flops might allow the realization of complex plasmonic circuits.

The authors acknowledge financial support by the Austrian Science Fund (SFB-ADLIS, SFB-IRON), the Austrian Nano Initiative project (PLATON), the EC Program "POISE" (TRM), the Lithuanian State and Studies Foundation (contract No C-07004), and the Society for Microelectronics (GME, Austria).

- 
- <sup>1</sup> Le Nguyen Binh, *Photonic Signal Processing: Techniques and Applications* (CRC Press, FL, USA, 2007).  
<sup>2</sup> E. Ozbay, *Science* **311**, 189 (2006).  
<sup>3</sup> A. Yariv, and X. Sun, *Opt. Express* **15**, 9147 (2007).  
<sup>4</sup> H. Park *et al.*, *Nature Photon.* **2**, 622 (2008).  
<sup>5</sup> J. Faist *et al.*, *Science* **264**, 553 (1994).  
<sup>6</sup> R. Köhler *et al.*, *Nature* **417**, 156 (2002).  
<sup>7</sup> C. Gmachl *et al.*, *Science* **280**, 1556 (1998).  
<sup>8</sup> G. Fasching *et al.*, *Appl. Phys. Lett.* **87**, 211112 (2005).  
<sup>9</sup> L. Mahler *et al.*, *Nature Photon.* **3**, 46 (2009).  
<sup>10</sup> E Mujagic *et al.*, *Appl. Phys. Lett.* in press.  
<sup>11</sup> H. Zhang *et al.*, *Opt. Express* **15**, 16818 (2007).  
<sup>12</sup> Y. Chassagneux *et al.*, *Nature* **457**, 174 (2009).  
<sup>13</sup> A. Benz *et al.*, *Opt. Express* **17**, 941 (2009).  
<sup>14</sup> M. Bayer *et al.*, *Phys. Rev. Lett.* **81**, 2582 (1998).  
<sup>15</sup> T. Mukaiyama *et al.*, *Phys. Rev. Lett.* **82**, 4623 (1999).  
<sup>16</sup> Y. P. Rakovich *et al.*, *Phys. Rev. A* **70**, 051801 (2004).  
<sup>17</sup> A. Nakagawa, S. Ishii, and T. Baba, *Appl. Phys. Lett.* **86**, 041112 (2005).  
<sup>18</sup> B. Williams *et al.*, *Appl. Phys. Lett.* **82**, 1015 (2003).  
<sup>19</sup> V. Tamošiūnas *et al.*, *Act. Phys. Pol. A* **107**, 179 (2005).  
<sup>20</sup> The Yee cell size was set to  $1.4 \mu\text{m}$  and the average relative dielectric constant of the heterostructure was set to 11.75 based on the better fitting of the spectra with earlier single cavity simulations.  
<sup>21</sup> C. Sirtori *et al.*, *IEEE J. Quantum Electron.* **34**, 1722 (1998).  
<sup>22</sup> J. Kröll *et al.*, *Nature* **449**, 698 (2007).